Cement & Concrete Composites 34 (2012) 370–376

Contents lists available at SciVerse ScienceDirect

Cement & Concrete Composites

journal homepage: www.elsevier.com/locate/cemconcomp

Size effect of concrete samples on the kinetics of external sulfate attack

Xavier Brunetaud [a,*], Mohammed-Rissel Khelifa [a,b], Muzahim Al-Mukhtar [a]

[a] University of Orléans, CRMD UMR 6619, 1 B rue de la Férollerie, 45071 Orléans Cedex 2, France
[b] University El-Hadj Lakhdar of Batna, 05000 Batna, Algeria

ARTICLE INFO

Article history:
Received 9 June 2010
Received in revised form 16 August 2011
Accepted 25 August 2011
Available online 13 September 2011

Keywords:
Size effect
Constant immersion
External sulfate attack
Ettringite
Non-destructive testing

ABSTRACT

The external sulfate attack (ESA) of concrete is a disease related to expansive sulfate hydrate formation in a hardened cement matrix. The aim of this research is to study how the choice of a concrete sample size can impact on the kinetics of ESA, by exposing different types of specimen to constant immersion in a solution dosed with 5% $Na_2SO_4{\cdot}10H_2O$. Monitoring involves mass, dynamic modulus and expansion measurements. It is concluded that 4×8 cm concrete cylinders (cored from 11×22 cm concrete cylinders) are more quickly damaged by ESA than usual sample types (11×22 cm concrete cylinders and $4 \times 4 \times 16$ cm mortar prisms). For all sample types, damage is always limited to the periphery of the sample in the short run. The thickness of the damaged zone is in the region of the size of the largest aggregates. For 4×8 cm concrete cylinders, this periphery corresponds to the entire sample because the maximum aggregate size is of the order of the size of the specimen. In this situation, the percolating crack network resulting from swelling is assumed to dramatically damage the cement matrix and to give sulfate solution access to the whole sample. Hence, by using this original type of cored samples, the concrete resistance to sulfate attack can be studied under reliable conditions (concrete formulations and not mortar ones, good sensitivity to ultrasonic tests) and advantage can be taken of the increased kinetics of degradation.

1. Introduction

Sulfate attack is due to the precipitation of secondary sulfate products, potentially high expansion and a chemo-mechanical deterioration [1]. Transport properties and strength are degraded by large cracking which is mainly visible at the paste/aggregate interfaces. This can lead to the destruction of the cementitious material. The induction period depends on the attack (type of aggressive agent, content and concentration of sulfates in contact) and cement used (type and water/cement ratio) [2]. Internal sulfate attack, or delayed ettringite formation (DEF), involves sulfates that are already present in the concrete. External sulfate attack (ESA), which is the subject of our study, involves a sulfate-rich external environment (i.e. presence of gypsum or pollution). The action of sulfate ions from gypsum as a retarder, does not present a danger to the concrete: as a matter of fact, the formed hydrate is expansive but crystallizes in a fresh and plastic cement paste that withstands the resulting deformations. However, if expansive hydrate formation occurs in a hardened matrix, the crystallization is constrained by the porosity, and generates tensile stresses in the matrix. With adequate liquid or gaseous intake, the sulfate can react with some of the hydrated phases of the concrete (including portlandite and hydrated calcium-mono-sulfo-aluminate AFm) to produce gypsum and/or secondary ettringite [3,4]. Both sulfate-related hydrates can contribute to the expansion and cracking of concrete [5], but there is no linear relation between the amount of hydrate formed and the resulting expansion [6]. In field concretes, especially if limestone filler has been added (PLC or SCC), thaumasite formation is sometimes associated with ESA [7–12]. However, Irassar [13] concluded that despite the fact that limestone filler provides the required calcium carbonate for thaumasite precipitation, this reaction is the last attack stage after gypsum and/or ettringite formation.

Sulfate attack may take a long time to damage concrete, especially in low W/C concretes. In order to accelerate the damage induced by sulfate attack, one solution is to apply an accelerated protocol by submitting the samples to a more aggressive environment. In such cases, the risk is to diverge from normal testing or from actual field conditions, and to promote irrelevant pathological behavior. An alternative is to increase the sensitivity of the material by changing the sample's dimensions. The aim of this research is to study how the choice of a concrete sample size can impact on the kinetics of ESA. To achieve this goal, we tested the resistance of different types of concrete and mortar samples to sulfate-rich environments, by applying a protocol of constant immersion in a solution containing 5% $Na_2SO_4{\cdot}10H_2O$.

* Corresponding author. Tel.: +33 2 38 49 40 52; fax: +33 2 38 41 73 29.
E-mail address: xavier.brunetaud@univ-orleans.fr (X. Brunetaud).
URL: http://www.crmd.cnrs-orleans.fr (X. Brunetaud).

0958-9465/$ - see front matter © 2011 Elsevier Ltd. All rights reserved.
doi:10.1016/j.cemconcomp.2011.08.014

Even if the experimental plan was exclusively applied to self compacted concretes (SCC), the conclusions can be extended to ordinary concretes since the main concrete parameters that affect ESA are the type of cement, the W/C ratio and mineral additives, and not superplasticizer itself. However, since poorly compacted concretes are particularly vulnerable to chemical attack [14], and since SCC do not require compacting, the behavior of field SCC may present less variability compared to compacted concretes.

2. Experimental method

2.1. Specimens

We conducted our study on four types of SCC and their equivalent mortars with two types of cements (CEM II/A 42.5 and CEM I 42.5 PM-ES sulfate-resistant) and two different W/C ratios (0.49 and 0.59), all made with crushed calcareous aggregates. Concretes made out of CEM I PM-ES (Type V cement according to ASTM C 150) were used as the reference as they cannot react with sulfate-rich environments. Mortars were obtained from concrete formulation by limiting the aggregate size to 2 mm. Details on the formulations are given in Table 1. The compressive strength measured on 11 × 22 cm concrete cylinders and 4 × 4 × 16 cm mortar prisms, and their porosity, are given in Table 2.

While both cements are in the same class (42.5), the compressive strength of the concrete made with CEM I was higher than the compressive strength of the concrete made with CEM II. Different porosities can partly explain the difference in mechanical performance (see Fig. 1). Mortars were far more porous than concretes; which was expected from a visibly high content of trapped air. We chose to apply the aging protocol on concrete cylinders whose size was less than 11 × 22 cm. The choice of this unusual size was initially motivated by the fact that smaller samples allow lighter handling, a saving in materials and offering more rapid drying and water saturation. For this purpose, 4 × 8 cm cylinders were collected by coring from 11 × 22 cm cylinders (see Fig. 2) after 28 days of curing in water. We checked that the compressive strengths of the 11 × 22 cm cylinders were identical to those of the 4 × 8 cm cylinders.

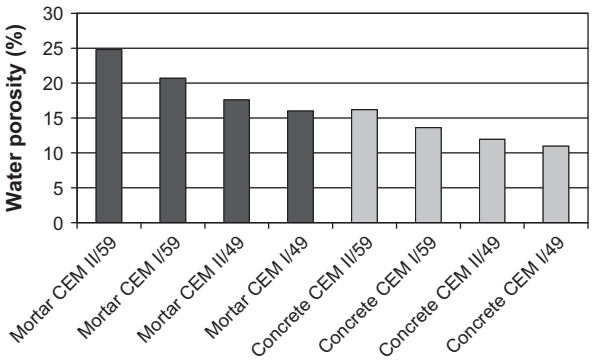

Fig. 1. Sample porosity in the unaltered state.

2.2. Aging protocol and specimen monitoring

Construction on wet gypsy soils or the immersion of the infrastructure in water polluted by sulfates allows the development of external sulfate attack [15–17]. The protocol applied in this study was a constant immersion in saline solution dosed with 5% $Na_2SO_4{\cdot}10H_2O$, renewed every 30 days. This protocol is most common in Ref. [18]; it typically simulates the case of concrete being attacked by sulfates through soil pollution such as gypsy soils.

Each specimen was monitored once per week:

- The mass change resulted in a gradual weight gain, while a loss of material caused by local ruptures greatly decreased the mass.
- The speed of propagation of non-destructive ultrasound evaluated the evolution of mechanical properties of the concrete since the velocity is correlated with the dynamic modulus. A drop in dynamic modulus reflects overall damage to the concrete.
- Linear expansion, only measured on mortar specimens, quantifies the swelling.
- A visual inspection of cracking assessed the degree of damage to the tested sample, and can be used in the diagnosis of the degradation.

Table 1
Formulation of the different SCC.

SCC	SCC_{01}: CEM II/59	SCC_{02}: CEM I/59	SCC_{03}: CEM II/49	SCC_{04}: CEM I/49
C (350 kg/m^3)	CEM II/A 42.5	CEM I 42.5 sulfate-resistant	CEM II/A 42.5	CEM I 42.5 sulfate-resistant
Sand 0/5 (kg/m^3)	922	922	971	971
Agg. 5/8 (kg/m^3)	262	262	275	275
Agg. 8/15 (kg/m^3)	602	602	633	633
Superplasticizer	1.4%	1.1%	2.0%	1.6%
Colloidal agent	0.05%	0.05%	/	/
Water/cement	0.59	0.59	0.49	0.49
Slump flow (cm)	58	60	74	68

Table 2
Mechanical performance and porosity of the different SCC and mortars.

SCC	SCC_{01}: CEM II/59	SCC_{02}: CEM I/59	SCC_{03}: CEM II/49	SCC_{04}: CEM I/49
R_{c7} (MPa)	15.6	24	23.3	32.8
R_{c28} (MPa)	18.8	27.9	29.6	38.0
Mortars	M_1: CEM II/59	M_2: CEM I/59	M_3: CEM II/49	M_4: CEM I/49
R_{f7} (MPa)	1.4	1.9	1.6	2.4
R_{f28} (MPa)	1.7	2.5	2.0	2.7
R_{c7} (MPa)	16.8	26.0	20.6	42.0
R_{c28} (MPa)	21.4	28.3	26.5	49.1

R_c = compressive strength; R_f = flexural strength.

Fig. 2. Coring of 4 × 8 cm cylinders from 11 × 22 cm cylindrical concrete specimens.

Fig. 3. Visual inspection of CEM II/59 11 × 22 cm cylinders after 5 months.

Non-destructive testing was realized through the measurement of the time of flight of ultrasound, performed with a Pundit+ which uses transducers at 83 kHz. The speed of propagation of ultrasound is calculated by dividing the length of the sample by the measured time of flight. The dynamic modulus is estimated by the velocity of the ultrasound using the following approximate relationship: $Edyn = V^2 \cdot \rho$ where Edyn is the dynamic modulus in N/m^2, V is the velocity in m/s and ρ is the density in kg/m^3.

Further analyses were performed to assess in greater detail the initial state of the samples or changes in their exposure to the aggressive environments. The total porosity was determined for all samples after complete drying at 60 °C and imbibition under vacuum conditions. SEM observations were performed on fracture fragments corresponding to the core of the samples. The fracture surface to be analyzed is fixed on a plot using a conductive adhesive and then brushed with silver paint on the sides prior to its carbon metallization. The samples were then observed using secondary electrons (SE), with an accelerating voltage of 5 kV.

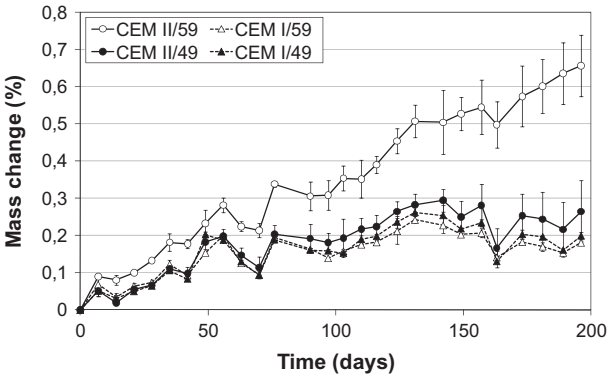

Fig. 4. Mass change of 11 × 22 cm concrete cylinders.

3. Experimental results

3.1. 11 × 22 cm concrete cylinders

Cylinders (11 × 22 cm) subjected to complete immersion showed no sign of degradation until the 5th month. From the 6th month, CEM II/59 and CEM II/49 samples underwent significant cracking along their circular ridge. For the same CEM II/A cement, the cracking of CEM II/59 (i.e. W/C = 0.59) was more pronounced compared to those of CEM II/49 (i.e. W/C = 0.49). Cracking was always located near the edges (see Fig. 3). The 11 × 22 cm cylinders of the concretes made with CEM I 42.5 PM-ES cement remained intact, regardless of the W/C, and no cracking was observed.

From Figs. 4 and 5, it can be seen there was a significant increase in mass and decrease in dynamic modulus for the 11 × 22 cm cylinders of CEM II/59. We also noted a slight mass increase, nonetheless significant for the samples of CEM II/49 concrete, which was only detectable from the 5th month. The mass and dynamic modulus of the specimens of CEM I/59 and CEM I/49 concrete did not undergo any significant variation.

3.2. 4x × 8 cm concrete cylinders

Fig. 6 shows the macroscopic consequences of immersion applied to the 4 × 8 cm cylinders of CEM II/59 concrete. From the third month, the visual aspect of the samples of CEM II/59 concrete revealed surface cracking corresponding to large cracks at the paste/aggregate interfaces, with particular swelling located at the ends of the samples, which is the most exposed area. The 4 × 8 cm cylinders of CEM II/49 concrete also suffered cracks, but in a less pronounced manner. For CEM II/49 specimens, 5 months were required to obtain the same level of degradation as with CEM II/59 specimens at 3 months.

Samples of CEM II/59 and II/49 were damaged until rupture, while samples of CEM I/59 and I/49 remained intact. For CEM II specimens, there was a significant decrease in the dynamic modulus with a significant increase in the mass and a visible swelling of the most exposed surface of the samples (Figs. 7 and 8). These symptoms were similar to those involved in a swelling reaction [1]. As aggregates are exclusively limestone, we could not determine any alkali-aggregate reaction (AAR).

3.3. 4 × 4 × 16 cm prismatic mortars

The mortars that were damaged by immersion were also the CEM II/49 and CEM II/59 specimens. The damage started at the 4th month for the CEM II/59 mortar and the 5th month for the CEM I/49 mortar (see Fig. 9).

Changes in mass and expansion (see Figs. 10 and 11) confirmed that there was a weight increase and a significant expansion for both mortars made from CEM II, particularly that with a high W/C (i.e. CEM II/59). The sharp falls of material were a bit smaller

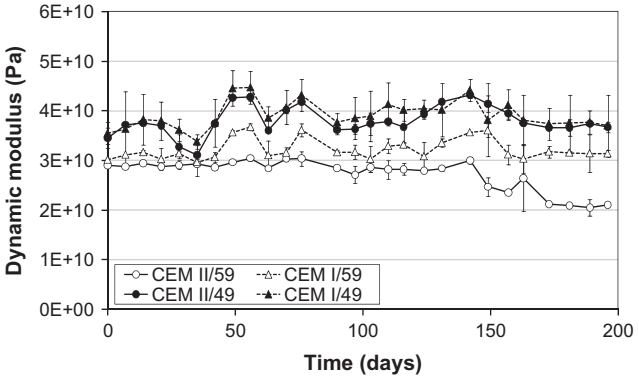

Fig. 5. Dynamic modulus of 11 × 22 cm concrete cylinders.

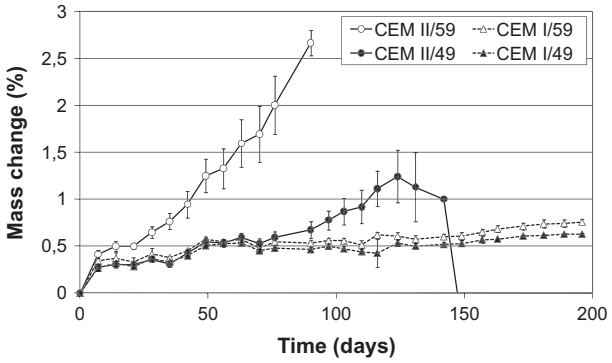

Fig. 7. Mass change of the 4 × 8 cm cylinders.

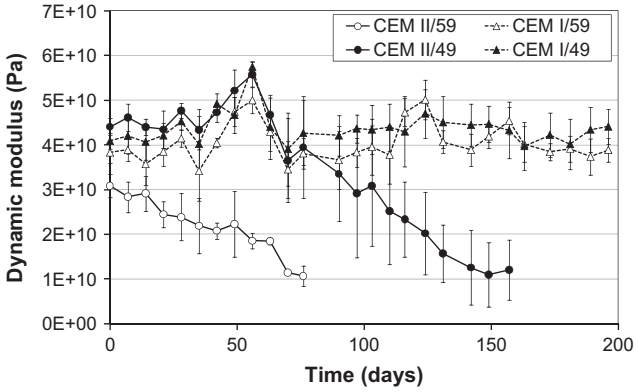

Fig. 8. Dynamic modulus of the 4 × 8 cm cylinders.

for mortars than for the 4 × 8 cm cylinders of concrete. We also noted a significant fall in the dynamic modulus for CEM II mortars (Fig. 12). This effect started at about 150 days for the CEM II/59 mortar, when expansion reached about 0.1%, which is consistent with previous studies [2]. For CEM I/59 and CEM I/49 mortars, no degradation was diagnosed.

3.4. SEM observations

SEM observations were conducted on the core of the 4 × 8 cm concrete cylinders (Fig. 13a, c, e) and the 4 × 4 × 16 cm mortar prisms (Fig. 13b, d, f) in order to compare the resulting microstructures after exposure to constant immersion in sulfate solution.

The micrographs of CEM II/59 4 × 8 cm cylinders showed the specific form of the ettringite rods, and high density stacking crystals at the paste/aggregate interface (see the center of Fig. 13a). In the case of CEM II/49 4 × 8 cm cylinders (Fig. 13c), the formation of ettringite is prevalent in the paste, and shows dense and massive crystallization. In both cases, no portlandite can be found in the vacuoles or in the ITZ. These microstructure changes prove that CEM II/59 and CEM II/49 4 × 8 cm concretes exposed to immersion were damaged by ESA to the core. CEM I/59 cm cylinders (Fig. 13e) exposed to immersion showed well-defined small ettringite deposits in vacuoles, and portlandite. These results confirm that the use of this CEM I PM-ES sulfate-resistant cement prevents the formation of deleterious sulfate-related hydrated products.

SEM observations of the mortar differed from those made on the 4 × 8 cm cylindrical specimens. For mortars containing CEM II, the observations showed the presence of a relatively large quantity of ettringite in the numerous vacuoles and the presence of a few altered portlandite crystals (see Fig. 13b for CEM II/59 mortars and Fig. 13d for CEMII/49 mortars). These observations might be seen as signs of sulfate-related activity, rather than a diagnosis of significant ESA-related pathology. These numerous vacuoles stemmed from the large amount of trapped air in the mortars, as demonstrated by the high porosity of the mortar with respect to concrete (see Fig. 1). Samples observed by SEM were extracted from core fragments. These observations prove that the core of these mortar specimens remained broadly unaltered. Macroscopic observations (Fig. 9) show that mortars were mainly damaged in the two millimeter thick periphery, which is the size of the largest aggregate. Micrographs of CEM I/59 mortars showed no significant sign of sulfate activity: little quantity of well-defined ettringite crystals and a large quantity of portlandite (Fig. 13f).

4. Discussion

Concrete cylinders (11 × 22 cm) corresponded to the most common dimensions for concrete specimens. When submitted to immersion in sulfate solution, these specimens showed

Fig. 6. Visual inspection of CEM II/59 4 × 8 cm concrete cylinders after 3 months.

Fig. 9. Visual inspection of CEM II/49 mortar at the 4th month (a) and CEM II/49 mortar at the 5th month (b).

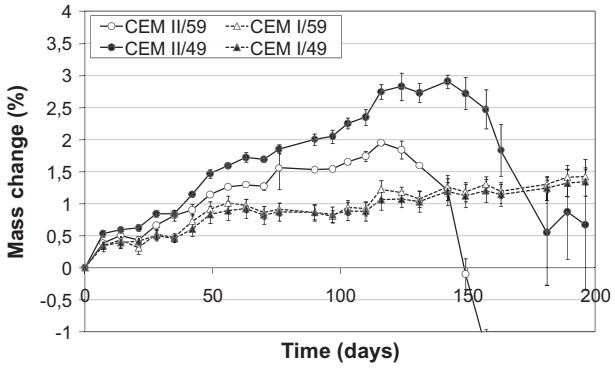

Fig. 10. Mass change of the 4 × 4 × 16 cm prismatic mortars.

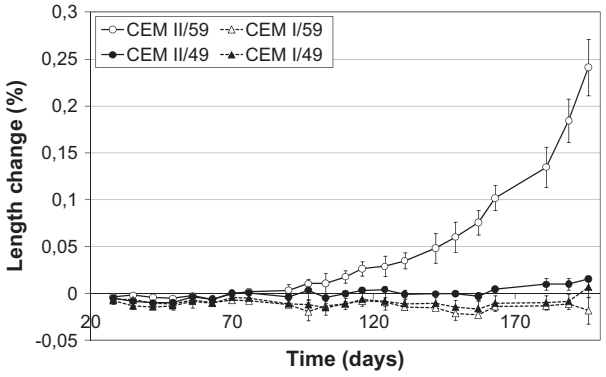

Fig. 11. Length change of the 4 × 4 × 16 cm prismatic mortars.

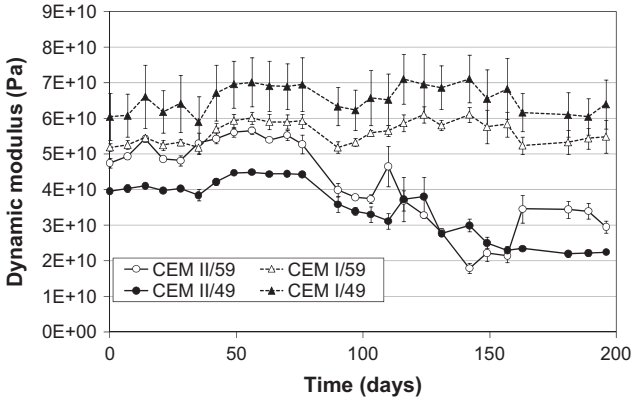

Fig. 12. Dynamic modulus of the 4 × 4 × 16 cm prismatic mortars.

macroscopic evidence of degradation after the 6th month on the more porous and less resistant samples (W/C = 0.59). Monitoring of W/C = 0.49 11 × 22 cm cylindrical specimens was pursued to ensure that they also became damaged, but this occurred later. For this type of specimen, dynamic modulus measurements were not particularly relevant since the core of the 11 × 22 cm cylindrical sample remained largely unaltered.

Mortar prisms (4 × 4 × 16 cm) corresponded to the most common dimensions for mortar specimens. When submitted to sulfates, these specimens showed macroscopic signs of ESA after 4 months for W/C = 0.59 specimens and 5 months for W/C = 0.49 specimens. As evidenced by SEM observation, the degradation was limited to the periphery of the sample, which represented, however, a larger fraction than in the context of the 11 × 22 cm concrete cylinders. This damage was concluded with a sudden drop in mass by surface fragmentation. The large amount of entrapped air in the mortars might have contributed to improve its resistance to sulfate attack. For this type of specimen, the use of measurement pins allowed monitoring the expansion of the sample, which corresponded to the most relevant criterion for judging the existence of a swelling reaction. For this geometry, dynamic modulus measurements were moderately sensitive since the core of the 4 × 4 × 16 cm prismatic sample was not as damaged as the surface.

Concrete cylinders (4 × 8 cm), obtained by coring into 11 × 22 concrete cylinders, were an original sample type. When submitted to the sulfate, the specimens showed macroscopic signs of ESA almost immediately for W/C = 0.59 and after 2–3 months for W/C = 0.49. This type of specimen was not equipped with measurement pins, it was not possible to simply and rigorously measure the expansion, only visual assessment was used to estimate swelling of around 10% located at the ends of the samples. Dynamic modulus measurements were very sensitive since the core of the 4 × 8 cm cylindrical sample quickly became damaged.

The accelerating effect of the 4 × 8 cm cylinders with respect to the 11 × 22 cylinders can be apportioned to the higher surface to volume ratio, since this ratio is twice as high for 4 × 8 cm as compared to 11 × 22 cm cylinders. Beyond this general effect, an interesting point is to take into account the actual surface in contact between the external sulfate solution and the cement matrix. Although calcareous aggregates are slightly porous (5%) and may contribute to the transport of sulfate solution, they do not react with sulfates and could be considered as non-reactive surfaces. The volumetric fraction of the calcareous aggregates (including sand) is about 67%. The resulting surface fraction of the cored specimens related to aggregate is quite high (see Fig. 6). As a

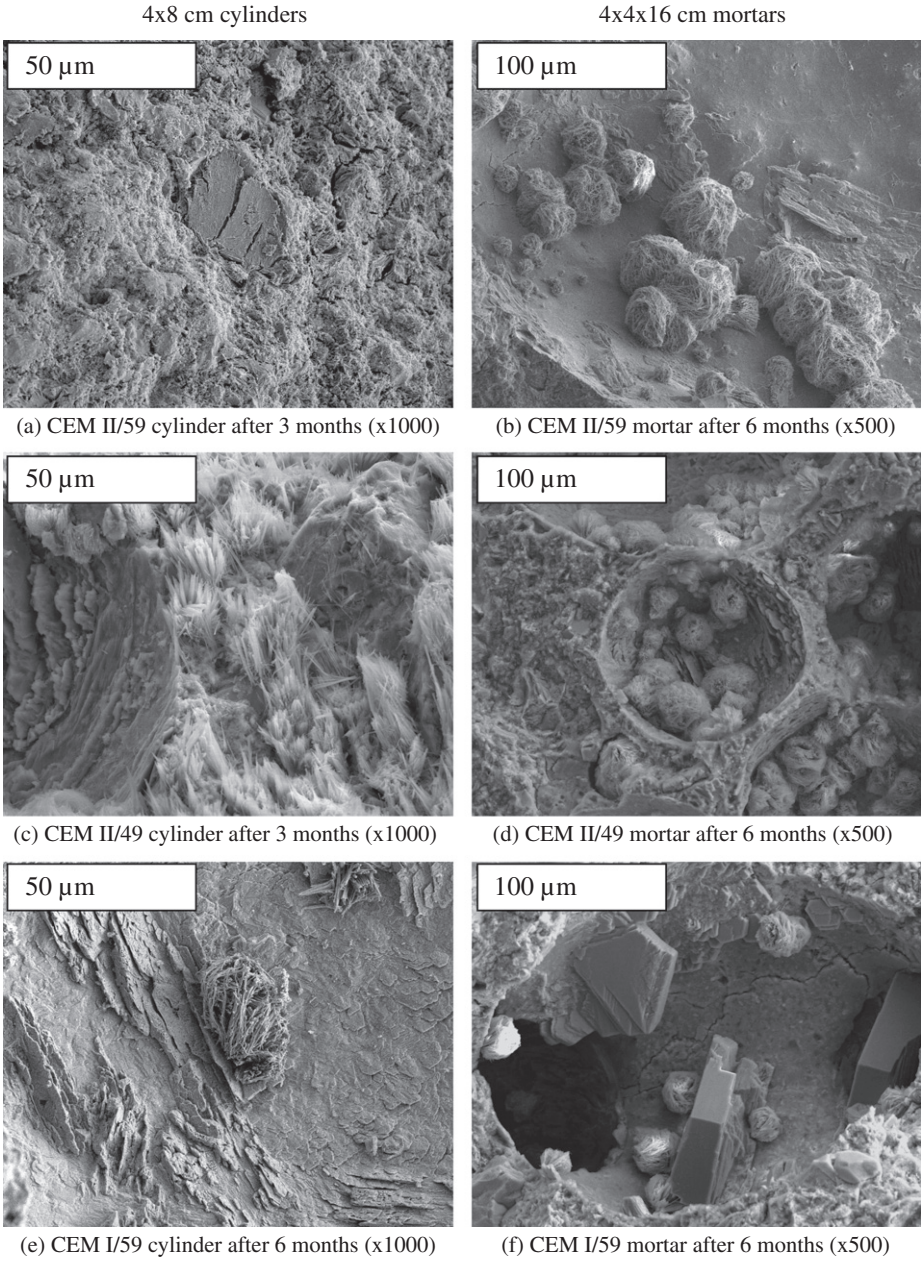

(a) CEM II/59 cylinder after 3 months (x1000) (b) CEM II/59 mortar after 6 months (x500)

(c) CEM II/49 cylinder after 3 months (x1000) (d) CEM II/49 mortar after 6 months (x500)

(e) CEM I/59 cylinder after 6 months (x1000) (f) CEM I/59 mortar after 6 months (x500)

Fig. 13. SE micrographs of core fractures, acceleration voltage of 5 kV.

consequence, the actual reactive surface to volume ratio may not be higher for cored specimens compared to usual 11×22 cm cylinders.

The accelerating effect may be assigned to a size effect related to the ratio of the smaller sample size to the size of the largest aggregates. This ratio is about 7.3 for 11×22 cylinders and 2.7 for 4×8 cylinders. This size effect hypothesis can also be applied to the comparison between 4×8 cm concretes and $4 \times 4 \times 16$ cm mortars. The reaction proceeded faster in concrete than in mortar, when the smaller sample size is 4 cm in both cases, whereas the surface to volume ratio is higher for $4 \times 4 \times 16$ cm mortars than for 4×8 cm concretes. For $4 \times 4 \times 16$ cm mortars, the ratio of the smaller sample size to the size of the largest aggregates is 40 as opposed to 2.7 for 4×8 cm cylinders. The phenomenon of swelling successive to sulfate attack (internal or external) is intimately linked with the size of the largest aggregates. Homogeneous swelling of the paste causes cracking at the paste/aggregate interfaces, which begins with the largest aggregates. As shown in recent modeling of cracking induced by sulfate attack [19], the first cracks are expected in the peripheral part of the sample, around the largest aggregates. When the sample size became similar in magnitude to the largest aggregate, there was no longer any robust area that could handle the tensile stresses and thus contain the swelling of the affected area. Moreover, the resulting percolating crack network provides external sulfate solution direct access to the depth of the sample, not only the peripheral part. This contributes to accelerating the ingress of sulfate ions.

5. Conclusions

The various results confirmed that concretes and mortars made using CEM I 42.5 PM-ES sulfate-resistant cement remained non

sensitive to ESA. These materials were used as a reference in our study. They confirm that the negative effects of exposure to sulfates results from the interaction between sulfates and phases related to the type of cement.

CEM II/59 and CEM II/49 concrete and mortar specimens showed clear signs of ESA. For these specimens, we observed surface cracking whose mesh is proportional to the size of the largest aggregates; an increase in mass with a simultaneous expansion of the material, until a sudden drop in mass due to fragmentation; and a fall in the dynamic modulus, which is significant since expansion the reaches 0.1%. Moreover, core-affected specimens showed that ettringite precipitates in a very specific form corresponding to large massive deposits with a constrained aspect.

The concrete with the lowest resistance to sulfates was CEM II/59, when compared to CEM II/49. Both are made out of the same cement but the difference in W/C changes their behavior. Samples with a W/C = 0.59 degraded faster and further than those of W/C = 0.49, which is due to the decrease in strength and resistance to the ingress of sulfate by diffusion [20–22]. Reducing the W/C from 0.59 to 0.49 significantly slowed down the kinetics of degradation, without avoiding it.

The most significant effect resulted from the sample size. For cored 4×8 cm cylindrical specimens, whose sample size is in the order of magnitude of the largest aggregate, the first macroscopic effect of swelling directly results in the creation of a percolating crack network. This global cracking is assumed to dramatically damage the hydrated cement matrix, and to provide external sulfate solution access to the whole sample. As a consequence, these 4×8 cm cored specimens are much more sensitive to sulfate attack compared to 11×22 cm concrete cylinders and $4 \times 4 \times 16$ cm mortar prisms. This new sample type may be used to study the behavior of concretes by taking advantage of relevant non-destructive testing and increased sulfate attack sensitivity.

Acknowledgements

The authors would like to thank Dr. Kévin Beck, Assistant Professor at the University of Orléans, CNRS-CRMD UMR 6619, for his useful help during the experimental campaign.

References

[1] Brunetaud X, Divet L, Damidot D. Impact of unrestrained delayed ettringite formation-induced expansion on concrete mechanical properties. Cem Concr Res 2008;38(11):1343–8.
[2] Brunetaud X, Linder R, Divet L, Duragrin D, Damidot D. Effect of curing conditions and concrete mix design on the expansion generated by delayed ettringite formation. Mater Struct 2007;40(6).
[3] Lothenbach B, LeSaout G, Gallucci E, Scrivener K. Influence of limestone on the hydration of Portland cements. Cem Concr Res 2008;38(6):848–60.
[4] Schmidt T, Lothenbach B, Romer M, Neuenschwander J, Scrivener K. Physical and microstructural aspects of sulphate attack on ordinary and limestone blended Portland cement. Cem Concr Res 2009;39:1111–21.
[5] Tian B, Cohen MD. Does gypsum formation during sulphate attack on concrete lead to expansion? Cem Concr Res 2000;30:117–23.
[6] Brown PW, Taylor HFW. The role of ettringite in external sulfate attack. Materials science of concrete: sulfate attack mechanisms. The American Ceramic Society; 1998 [p. 73–97, Special Volume].
[7] Crammond NJ. The thaumasite form of sulfate attack in the UK. Cem Concr Compos 2003;25(8):809–18.
[8] Thomas MDA, Rogers CA, Bleszynski RF. Occurrences of thaumasite in laboratory and field concrete. Cem Concr Compos 2003;25(8):1045–50.
[9] Diamond S. Thaumasite in orange county, Southern California: an inquiry into the effect of low temperature. Cem Concr Compos 2003;25(8):1161–4.
[10] Stark DC. Occurrence of thaumasite in deteriorated concrete. Cem Concr Compos 2003;25(8):1119–21.
[11] Mingyu H, Fumei L, Mingshu T. The thaumasite form of sulfate attack in concrete of Yongan Dam. Cem Concr Res 2006;36(10):2006–8.
[12] Ma B, Gao X, Byars EA, Zhou Q. Thaumasite formation in a tunnel of Bapanxia Dam in Western China. Cem Concr Res 2006;36(4):716–22.
[13] Irassar EF. Sulfate attack on cementitious materials containing limestone filler – a review. Cem Concr Res 2009;39:241–54.
[14] BRE Special Digest 1, Concrete in Aggressive Ground, Parts 1–4, Second ed., BRE Centre for Concrete Construction and Centre for Ground Engineering Remediation; 2003.
[15] Mehta PK. Concrete: structure, properties and materials. Prentice-Hall; 1986. pp. 105–169.
[16] Skalny J, Pierce JS. Sulphate attack issues, Proceedings of a Seminar on Sulphate Mechanisms, Quebec City, Quebec, Canada; 1998.
[17] Cohen MD, Mather B. Sulfate attack on concrete – research needs. ACI Mater J 1991;24(1):177–202.
[18] Ghrici M, Kenai S, Mansour MS, Kadri E. Some engineering properties of concrete containing natural pozzolana and silica fume. J Asian Archit Build Eng 2006;8.
[19] Idiart AE, López CM, Carol I. Chemo-mechanical analysis of concrete cracking and degradation due to external sulfate attack: a meso-scale model. Cem Concr Compos 2011;33:411–23.
[20] Rozière E, Loukili A, El Hachem R, Grondin F. Durability of concrete exposed to leaching and external sulphate attack. Cem Concr Res 2009;39:1188–98.
[21] Sahmaran M, Kasap O, Duru K, Yaman IO. Effects of mix composition and water–cement ratio on the sulphate resistance of blended cements. Cem Concr Compos 2007;29:159–67.
[22] Khatri RP, Sirivivatnanon V, Yang JL. Role of permeability in sulphate attack. Cem Concr Res 1997;27(8):1179–89.